



HAL
open science

Gold Nanoparticles Assembly on Silicon and Gold Surfaces: Mechanism, Stability and Efficiency in Diclofenac Biosensing

Maroua Ben Haddada, Maria Hübner, Sandra Casale, Dietmar Knopp, Reinhard Niessner, Michele Salmain, Souhir Boujday

► **To cite this version:**

Maroua Ben Haddada, Maria Hübner, Sandra Casale, Dietmar Knopp, Reinhard Niessner, et al.. Gold Nanoparticles Assembly on Silicon and Gold Surfaces: Mechanism, Stability and Efficiency in Diclofenac Biosensing. *Journal of Physical Chemistry C*, 2016, 120 (51), pp.29302-29311. 10.1021/acs.jpcc.6b10322 . hal-01411566

HAL Id: hal-01411566

<https://hal.sorbonne-universite.fr/hal-01411566>

Submitted on 7 Dec 2016

HAL is a multi-disciplinary open access archive for the deposit and dissemination of scientific research documents, whether they are published or not. The documents may come from teaching and research institutions in France or abroad, or from public or private research centers.

L'archive ouverte pluridisciplinaire **HAL**, est destinée au dépôt et à la diffusion de documents scientifiques de niveau recherche, publiés ou non, émanant des établissements d'enseignement et de recherche français ou étrangers, des laboratoires publics ou privés.

1
2
3
4
5
6
7
8
9
10
11
12
13
14
15
16
17
18
19
20
21
22
23
24
25
26
27
28
29
30
31
32
33
34
35
36
37
38
39
40
41
42
43
44
45
46
47
48
49
50
51
52
53
54
55
56
57
58
59
60

Gold Nanoparticles Assembly on Silicon and Gold Surfaces: Mechanism, Stability and Efficiency in Diclofenac Biosensing

Maroua Ben Haddada^{1,3}, Maria Huebner², Sandra Casale¹, Dietmar Knopp², Reinhard Niessner², Michèle Salmain³, and Souhir Boujday^{1,}*

¹ Sorbonne Universités, UPMC Univ Paris 6, CNRS, Laboratoire de Réactivité de Surface (LRS), F75005 Paris, France

² Chair for Analytical Chemistry and Institute of Hydrochemistry, Technical University Munich, Marchioninstr. 17, Munich, Germany

³ Sorbonne Universités, UPMC Univ Paris 06, CNRS, Institut Parisien de Chimie Moléculaire (IPCM), 4 place Jussieu F-75005 Paris, France

Laboratoire de Réactivité de Surface, UMR CNRS 7197, *Sorbonne Universités, UPMC Univ Paris 6, CNRS*, case 178, 4 Place Jussieu, 75252 Paris cedex 05, France

Tel: +33144276001, Fax: +33144276033, souhir.boujday@upmc.fr

1
2
3 ABSTRACT. We investigated the assembly of Gold nanoparticles (AuNPs) on Gold and Silicon
4 sensors with two final objectives: (i) understanding the factors governing the interaction and (ii)
5 building up a nanostructured piezoelectric immunosensor for diclofenac, a small-sized
6 pharmaceutical pollutant. Different surface chemistries were devised to achieve AuNPs assembly
7 on planar substrates. These surface chemistries included amines to immobilize AuNPs *via*
8 electrostatic interaction, or a mixture of amines and thiols to covalently attach the AuNPs. We
9 also generated PEG-amine terminated surfaces to benefit from the well-known non-biofouling
10 properties of PEG-coated surfaces. The functional substrates and the resulting gold nanoparticle
11 layers were characterized in detail by Surface IR, contact angle measurements and Scanning
12 Electron Microscopy (SEM). The mechanism of adsorption is discussed herein considering the
13 nature of the terminal groups and their charge at the pH of AuNPs adsorption. The coverage and
14 the dispersion of AuNPs were strongly dependent on the anchoring points on the surfaces; the
15 optimal were reached when the attachment layer offered multiple interaction points, in particular,
16 for NH₂/SH and PEG/NH₂ terminated surfaces, where the percentage of isolated particles was up
17 to 78 %. In addition, PEG-coated surfaces led to a stable AuNPs layer resistant to ultrasounds
18 and to further functionalization of the immobilized nanoparticles. These surfaces were used to
19 engineer quartz crystal microbalance (QCM) biosensors for diclofenac detection. The AuNPs
20 nanostructured substrates significantly enhanced the biosensor sensitivity as compared to planar
21 substrates (up to 6 times higher). This enhancement presages a higher sensitivity in the
22 competitive detection of diclofenac on these systems. More importantly, despite the
23 biorecognition and the drastic regeneration conditions, SEM images show that gold nanoparticles
24 layers are stable and reliable, which paves the way for their use as nanostructured platforms for
25 multiple applications.
26
27
28
29
30
31
32
33
34
35
36
37
38
39
40
41
42
43
44
45
46
47
48
49
50
51
52
53
54
55
56
57
58
59
60

1
2
3 INTRODUCTION
4

5 The assembly of gold nanoparticles (AuNPs) onto planar substrates has expanded tremendously
6 over the last several decades, particularly in the biosensors field¹⁻³. These nano-objects lead to
7 dramatic improvements in the performance and sensitivity of biosensing devices owing to their
8 plasmonic properties and to their efficiency as nanostructuring agents. The benefit from
9 plasmonic properties of planar substrates decorated by gold nanoparticles is dramatic for
10 techniques such as surface enhanced Raman spectroscopy (SERS) now widely employed for
11 biosensing⁴⁻⁶. The interest in these nano-objects for signal enhancement in biosensors based on
12 non optical techniques is more recent, yet it is growing fast. In the particular case of quartz
13 crystal microbalance (QCM) biosensors, nanostructuring of the surface of the quartz crystal
14 electrodes with AuNPs leads to an increase of the accessible surface area and by then the number
15 of binding sites⁷⁻⁸. For DNA biosensors, nanostructuring by AuNPs results in a better
16 attachment of the oligonucleotides to the surface, up to 10 times higher than on planar substrates,
17 and therefore an increased capacity for nucleic acid detection⁹⁻¹¹. The same trend was observed
18 for antibody-based biosensors; despite the bigger size of these receptors, their density was
19 improved while preserving affinity to their target¹²⁻¹⁴. All the same, antibody fragment based
20 biosensors benefit from AuNPs assembly; higher sensitivity and overall better immunosensing
21 performances were evidenced¹⁵⁻¹⁶.

22 Grafting of metallic particles on substrates is often done *a posteriori*, starting from colloidal
23 solutions⁴. Commonly synthesized by the so-called “Turkevich Synthesis¹⁷,” –involving the
24 reduction of Au ions by reducing agents such as citrate – gold nanoparticles are formed through a
25 classical nucleation and growth process terminated by citrate ($\text{Na}_3\text{C}_6\text{H}_5\text{O}_7$), which controls the
26 nanoparticle size and morphology by acting as a surface functional layer or a capping agent, and
27
28
29
30
31
32
33
34
35
36
37
38
39
40
41
42
43
44
45
46
47
48
49
50
51
52
53
54
55
56
57
58
59
60

1
2
3 preventing inter-particle aggregation through electrostatic repulsion. Prior to AuNPs deposition,
4
5 surfaces need to be covered with reactive functions, usually amines or thiols, to favour the
6
7 interaction with AuNPs through electrostatic or covalent bonds. Molecules commonly used at
8
9 this step are organothiols in the case of gold¹⁸⁻¹⁹ or organosilanes for oxidized silicon and glass
10
11 surfaces²⁰⁻²¹. More recently, polymer-based coating was applied to attach AuNP on planar
12
13 substrates²²⁻²³. Poly(ethylene glycol) (PEG) is particularly adapted to biosensing applications by
14
15 forming smooth and uniform PEG films that inhibit non specific adsorption²⁴⁻²⁵ and provide a
16
17 high affinity to citrate-stabilized gold nanoparticles²⁶⁻²⁷. Once AuNPs are immobilized on a
18
19 substrate, although the citrate capping agent is well-suited as a native functional layer during
20
21 synthesis, substituting citrate, which is only bound loosely to the nanoparticle surface through
22
23 weak van der Waals interactions, by a more tightly bound and well-defined capping layer is
24
25 mandatory for further grafting of biomolecules or target and application in biosensing. For this
26
27 post-functionalization the organosulfur compounds represent perhaps the most widely practiced
28
29 route²⁸⁻²⁹. To withstand this post-functionalization, AuNP layers should also be stable over time
30
31 and their interaction with the surface strong enough to ensure that the nanoparticles remain
32
33 attached during further functionalization and upon utilization. Despite the huge interest in AuNP-
34
35 nanostructured substrates, the assembly of gold nanoparticles on surfaces and their post-
36
37 functionalization still rely on an approximate approach since the fundamentals of the chemistry
38
39 involved in the adsorption process are poorly understood^{20, 30-31}.

40
41 In this contribution, we investigated the mechanism of assembly and the stability of spherical
42
43 gold nanoparticles on functionalized silicon and gold substrates. To this purpose, we devised
44
45 different surface chemistries to establish the key-parameters in the attachment layer that
46
47 dominate the interaction with gold nanoparticles. Both gold and oxidized silicon substrates were
48
49
50
51
52
53
54
55
56
57
58
59
60

1
2
3 modified by thiols and silanes to generate amine-terminated layers. Then, reaction of a thiol-
4 terminated carboxylic acid with the grafted amines allowed us to generate mixed thiol/amine
5 terminated layers. In addition, we utilized diamine-PEG cross-linked to acid and epoxy groups
6 on gold and silicon, respectively, to compare the efficiency of these films to the previous ones.
7
8 The assembly of gold nanoparticles on these platforms was examined in depth by Scanning
9 Electron Microscopy (SEM), focusing on the coverage and dispersion, and the impact of the
10 attachment layers is discussed. We also investigated the influence of the post-functionalization
11 agent (either an organothiol or a PEG) on the AuNP layers. Finally, the stable and well-dispersed
12 layers are used to build piezoelectric immunosensors for the anti-inflammatory drug diclofenac
13 and their efficiency was compared to planar surfaces. The stability of AuNP layer upon
14 biorecognition and regeneration processes was eventually investigated by SEM.
15
16
17
18
19
20
21
22
23
24
25
26
27
28
29
30
31
32
33

34 EXPERIMENTAL SECTION

35
36 **Materials:** Sodium citrate, gold(III) chloride trihydrate, 3-glycidyloxypropyltrimethoxysilane
37 (GOPTS), tannic acid, N-ethyl-N'-(3-(dimethylamino)propyl)carbodiimide hydrochloride (EDC),
38 cysteamine.HCl (CEA), diclofenac sodium salt, phosphate-buffered saline (PBS) pH= 7.4,
39 poly(ethylene glycol) bis(amine) DAPEG₆₈ (MW= 3000 Da) , N-hydroxysuccinimide (NHS),
40 11-mercaptoundecanoic acid (MUA), (3-aminopropyl)triethoxysilane (APTES) (99%), silicon
41 wafers <111> and anti-mouse IgG (Fc specific) antibody produced in goat were purchased from
42 Sigma–Aldrich. Poly(ethylene glycol) bis(amine) DAPEG₄₅ (MW = 2000 Da) was obtained from
43 Huntsman (Rotterdam, Netherlands). Sodium dodecyl sulfate (SDS) was purchased from Fisher
44 Scientific. The rabbit polyclonal anti-diclofenac serum was prepared in-house³², its analytical
45
46
47
48
49
50
51
52
53
54
55
56
57
58
59
60

1
2
3 potential is detailed in reference ³³. Milli-Q water (18 MΩ, Millipore, France) was used for the
4
5 preparation of the solutions and for all washes. Experiments were carried out at room
6
7 temperature unless otherwise stated.
8
9

10
11
12 **Surface chemistry:** Silicon wafers cut into 1 x 1 cm pieces were cleaned following a procedure
13 including several washing steps and treatment by hydrochloric acid / methanol 1:1 (v/v) for 1 h.
14
15 Reactive hydroxyl groups were generated by shaking wafers in sulfuric acid for 1 h. After
16
17 washing with water, the substrates were dried under nitrogen flow ³⁴. APTES was grafted by
18
19 immersing the wafers in a solution of silane in anhydrous toluene (50 mM) and heating at 75°C
20
21 for 24 h. Samples were washed twice, sonicated for 10 min in anhydrous toluene, dried under
22
23 nitrogen flow, and heated at 90°C for 2 h ³⁵. Surface sulfhydryl functions were generated by
24
25 exposing the wafers to a solution of MUA (10 mM in EtOH previously activated with NHS (2.4
26
27 eq.) and EDC (1.2 eq.)). Grafting of GOPTS was carried out by covering wafers with GOPTS
28
29 (100 μL) and avoiding exposure to the atmosphere by assembling two substrates face-to-face.
30
31 After 3 h, the sandwiches were separated and sonicated first in ethanol, then in methanol and
32
33 again in ethanol for 5 min each. They were dried under nitrogen flow and heated for 5 min at
34
35 85°C. Afterwards, the wafers were treated with molten DAPEG₄₅ (600 μL) and incubated at
36
37 98°C for 12 h in the sandwich format. The wafers were separated, sonicated in water for 15 min
38
39 and dried under nitrogen flow ²⁵.
40
41
42
43
44
45
46
47

48 Gold-coated sensors were immersed in a freshly prepared solution of CEA (10 mM in water) or
49
50 MUA (10 mM in EtOH) for 18–24 h. After washing with the same solvent, the CEA-treated
51
52 surfaces were dipped into a solution of MUA (10 mM in EtOH previously activated with NHS
53
54 (2.4 eq.) and EDC (1.2 eq.)) for 2 h. The MUA-treated surfaces were exposed to 150 μL of an
55
56
57
58
59
60

1
2
3 aqueous solution of NHS (2.4 eq.) and EDC (1.2 eq.) for 2 h to activate the carboxyl groups. The
4
5 surfaces were rinsed with the same solvent and dried under nitrogen flow. DAPEG₄₅
6
7 immobilization was finally performed as described above. All the functional substrates were
8
9 stored in a dessicator.
10
11

12
13
14
15 **Gold nanoparticles preparation and deposition:** Colloidal gold particles were prepared
16
17 according to the tannic acid method of Slot and Geuze³⁶. To produce 100 mL of a 14 nm
18
19 diameter colloid solution, two stock solutions were prepared: solution A: 1 mL 1% (w/v) HAuCl₄
20
21 and 79 mL water; solution B: 4 mL 1% sodium citrate, 0.025 mL 1% tannic acid and 16 mL
22
23 water. Solutions A and B were heated to 60°C under stirring then mixed. When the solution
24
25 turned red, the mixture was heated up to 95°C for a few minutes and cooled on ice. Colloidal
26
27 solutions were kept in amber glassware, stored in the refrigerator at 4°C and used within a
28
29 month. Modified substrates were dipped into the prepared colloid solution, with no further
30
31 dilution for 90 min under sonication (Elma, 90 W, 45 kHz), washed twice in water and dried
32
33 under nitrogen. Surfaces were finally immersed in a solution of CEA or DAPEG₆₈ (1mM in
34
35 EtOH) for 2 h to decorate the AuNPs with amino groups. The resulting substrates were stored in
36
37 a dessicator.
38
39
40
41
42
43
44

45
46 **Covalent grafting of Diclofenac:** Diclofenac (10 mM in dry DMF) was activated by treatment
47
48 with NHS (1.2 eq.) and EDC (1.2 eq.) for 150 min at room temperature. Then, the substrates
49
50 terminated by amino groups were dipped into the solution, shaken over night at room
51
52 temperature, washed for 15 min in water and dried under nitrogen flow. They were stored in a
53
54 desiccator.
55
56
57
58
59
60

1
2
3 **Binding of anti-diclofenac antibody:** The mixture of PBS and ethanol 9:1 was thoroughly
4 degassed under vacuum (for 15 min) and used as carrier buffer in the flow system (flow rate
5 25 $\mu\text{L min}^{-1}$). The sequence of injections was carried out as follows:
6
7

8
9
10 10-20 min flow of carrier buffer to stabilize the baseline signal; 10 min flow of 1/500 dilution of
11 anti-diclofenac serum in PBS/EtOH; Washing with carrier buffer
12
13

14
15 The regeneration buffer was a solution of 2 w% sodium dodecyl sulfate (SDS) in water/ethanol
16 (9/1=v/v) at pH=2 (HCl).
17
18
19

20
21
22 **Characterization techniques:** Transmission Electron Microscopy (*TEM*) measurements were
23 performed using a JEOL JEM 1011 microscope operating at an accelerating voltage of 100 kV.
24
25

26
27 The TEM grids were prepared as follows: Typically 1.5 mL of the colloid solution was
28 centrifuged at 11200 g for 10 min to precipitate the particles. The colorless supernatant was
29 discarded. The residue was re-dispersed in a suitable volume of water. 2 μL of this particle
30 suspension was dispensed on a carbon-coated copper grid and dried at room temperature. Gold
31 nanoparticles size distribution was determined using ImageJ. Scanning Electron Microscopy
32 (*SEM*) of the gold and silicon substrates covered with AuNPs was performed using a FEG SU-
33 70 scanning electron microscope with a low voltage of 1 kV at a distance of 1.9 - 2.3 mm; the
34 secondary electron detector "in Lens" was used. Images taken at different scales and in different
35 regions of the samples were recorded. The particle densities were calculated by counting the
36 particles in the SEM images (isolated and aggregates of 2, 3, 4, 5, 6, and > 6 particles) on a
37 representative area of 2.3 – 2.5 μm^2 . For **Contact Angle measurements** static water contact
38 angles were measured at room temperature using the sessile drop method and image analysis of
39 the drop profile. The instrument, which uses a CCD camera and an image analysis processor, was
40
41
42
43
44
45
46
47
48
49
50
51
52
53
54
55
56
57
58
59
60

1
2
3 purchased from Krüss Optronic GmbH (Hamburg, Germany). The water droplet volume was 1
4
5 μL , and the contact angle (Θ) was measured 5 s after the drop was deposited on the sample. For
6
7
8 each sample, the reported value is the average of the results obtained on 3 droplets and the
9
10 overall accuracy in the measurements was better than $\pm 5^\circ$. ***PM-IRRAS*** spectra were recorded on
11
12 a commercial NICOLET Nexus FT-IR spectrometer. Details on the experimental set-up are
13
14 available in reference ³⁷. Sensor chips were made of borosilicate glass substrates (11 mm \times 11
15
16 mm), coated successively with a 2.5 ± 1.5 nm thick layer of chromium and a 250 ± 50 nm thick
17
18 layer of gold (Arrandee, Werther, Germany). They were annealed in a butane flame to ensure a
19
20 good crystallinity of the topmost layers and dipped in a bath of absolute ethanol during 15 min
21
22 before adsorption. The Si wafers were analyzed by ***GA-ATR-IR*** immediately after their
23
24 preparation. GA-ATR-IR spectra (256 scans, 4 cm^{-1} resolution) were recorded on a Tensor 27
25
26 spectrometer (Bruker) equipped with a VariGATR accessory (Harrick Scientific, Pleasantville,
27
28 NY) and incidence angle set at 60° . Quartz Crystal Microbalance with dissipation measurements
29
30 (***QCM-D***) were carried out with a 4-channel dissipative quartz crystal microbalance (Q-Sense
31
32 E4) using AT-cut 5 MHz quartz crystals (QCM sensors, 14 mm diameter) coated with a 3-100 nm
33
34 layer of gold or a 50 nm SiO_2 film (Lot-oriel) at 22°C . Prior to use, they were cleaned by ethanol
35
36 and dried under nitrogen flow. Experiments were carried out in flow-through conditions using a
37
38 peristaltic pump. Data were simultaneously acquired at the fundamental frequency F of 5 MHz
39
40 ($N = 1$) and several overtone frequencies (15, 25, 35, 45, and 55 MHz, i.e. $N = 3, 5, 7, 9$ and 11).
41
42
43
44
45
46
47
48 Two physical parameters are discussed: the resonance frequency and the dissipation. The
49
50 frequency change can be correlated to the mass of the adsorbed layer using the Sauerbrey
51
52 equation ³⁸: $\Delta F = - N \Delta m / C_f$, where C_f ($= 17.7 \text{ ng cm}^{-2} \cdot \text{Hz}^{-1}$ at $F = 5 \text{ MHz}$) is the mass-
53
54 sensitivity constant, and N is the overtone number.
55
56
57
58
59
60

RESULTS AND DISCUSSION

Synthesis and characterization of AuNPs: Citrate-stabilized spherical AuNPs were selected for this work as their synthesis has reached a level of maturity allowing a precise control of their shape, size, and dispersion. The size and dispersion of the gold colloids prepared in this work were estimated from UV-visible spectroscopy and Transmission Electron Microscopy (TEM) analyses. UV-Vis spectra and TEM images are given in the supplementary material section. On the UV-Vis spectrum (Figure S1-a), a narrow resonance plasmon band was present at 520 nm, typical of a particle size around 15 nm³⁹⁻⁴⁰. This was confirmed by TEM images (Figure S1-b), mathematical treatment of the images showed a homogeneous particle size distribution with an average size of 13.5 ± 1 nm. The AuNP concentration in the solution, estimated by two methods (see supplementary section) was 3.6 ± 0.2 nmol L⁻¹.

Surface functionalization of Au and Si substrates: Six different surface chemistries were devised to generate a layer of AuNPs on gold and silicon planar substrates as schematized in Figure 1. Adhesion layers either included amines to ensure a strong electrostatic interaction with citrate-stabilized AuNPs⁴¹ or amines and thiols to covalently bind AuNPs through S-Au bonds. In addition, adhesion layers including NH₂-terminated poly(ethylene) glycol) were built up to benefit from the well-known anti-biofouling properties of PEG-coated surfaces and prevent non specific adsorption during the immunosensing process²⁷. We used a diamine-PEG (DAPEG₄₅) with a molecular weight of 2,000 Da, since this medium size PEG has been previously shown to provide a homogeneous cover on Si wafers^{24, 26, 42}.

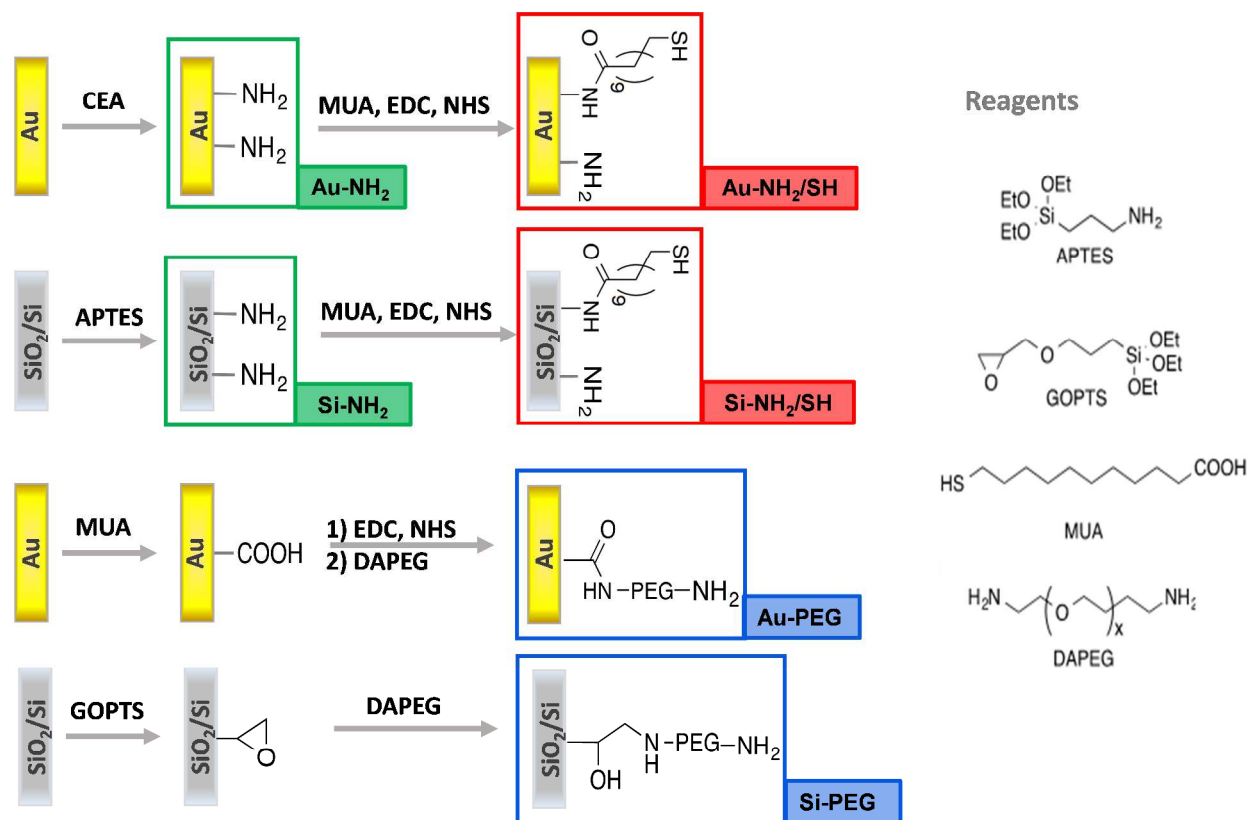


Figure 1 Surface functionalization strategies devised for immobilization of AuNPs on gold and silicon substrates and adopted nomenclature for substrates.

Amine-terminated surfaces were generated on gold and silicon using CEA and APTES, respectively. Mixed amine/thiol terminated layers were obtained by reacting MUA on the previous amine-terminated layers. MUA reacts with approx. 24 % of amine groups leading to layers with SH/NH₂ ratio ~1/4²⁰. Amine-terminated PEG layers were built up by conjugating DAPEG to carboxy-decorated gold and epoxy-decorated silicon substrates that had been obtained by self-assembling of MUA and GOPTS, respectively (see Figure 1). The terminal carboxylic acid groups of MUA SAM on gold were converted into NHS esters by reaction with EDC and NHS prior to DAPEG grafting according to a previously published procedure²⁵. The resulting surfaces are named according to the following nomenclature: Substrate (Au or Si) –

Terminal group (NH₂, NH₂/SH, or PEG) as depicted in Figure 1.

Prior to AuNPs immobilization, the functionalized substrates were characterized by contact angle measurements and surface IR. Table 1 summarizes the static water contact angle values measured for these substrates.

Table 1 Static water contact angle measurements

	Si		Au	
Clean	< 10°		46±2°	
1 st layer	APTES	GOPTS	CEA	MUA
	83±2°	51±1°	51±2°	59±2°
2 nd layer	APTES+MUA	PEG	CEA+MUA	PEG
	40±4°	43±2°	48±1°	40±4°

The initial clean (oxidized) silicon surface was very hydrophilic as expected by the strong oxidizing conditions applied to the samples before analysis to generate a high density of surface hydroxyl groups²⁵. Silanization with APTES resulted in a very large increase of the contact angle from 15° to 83° due to the presence of more or less ordered aminopropyl chains^{35,43}. Further covalent binding of MUA resulted in a drop of the contact angle to 40°. This increase of hydrophilic character may result from a better packing of the organic layer owing to Van der Waals forces between the longer hydrocarbon chains of MUA⁴⁴. Silanization with GOPTS also led to an increase of contact angle from 15 to 51° as a result of organic group presence on the surface. Treatment with DAPEG slightly decreased the contact angle to 43° in agreement with the known hydrophilic character of PEG derivatives²⁶. The same trend was observed for gold surfaces, i.e. an increase of the contact angle upon CEA or MUA grafting⁴⁵ and a decrease after DAPEG grafting consistent with the higher hydrophilic character expected for PEG-covered surfaces. The contact angle measured for Au-PEG was roughly the same as the one measured for Si-PEG, ~ 40°.

Surface IR, either in ATR mode for silicon substrates, or PM-IRRAS mode for gold substrates,

1
2
3 was used to characterize the molecular composition of the thin films deposited on both surfaces.
4
5 The recorded spectra are shown in the supplementary information section (Figures S2, 3, and 4)
6
7 together with the detailed band attributions (table S2). Briefly, for both substrates the
8
9 characteristic bands expected upon surface modification were observed. On Au-NH₂ and Si-NH₂
10
11 the primary amine bands were present in the range 1660–1640 cm⁻¹ the ammonium group bands
12
13 around 1480 and 1571 cm⁻¹. Upon MUA grafting the intensity of these bands was lower and
14
15 amide bands appeared giving evidence of the successful conjugation of activated acid to surface
16
17 amine groups. All the same, successful grafting of DAPEG on Au-MUA and Si-GOPTS
18
19 substrates was evidenced on both systems by the presence in the IR spectra of an intense band at
20
21 1110 cm⁻¹, assigned to the intense C-O-C stretching mode of the PEG chains^{25, 46}.
22
23
24
25
26
27
28

29 **Gold nanoparticles immobilization on functionalized surfaces:** The AuNPs layer attachment
30
31 to the surface must be strong enough to prevent desorption/release during the successive steps of
32
33 biosensor elaboration, test and regeneration. Therefore, ultrasounds were applied during AuNP
34
35 deposition, to remove loosely bound nanoparticles. In addition, we have previously observed that
36
37 applying ultrasounds during deposition of AuNPs on Si surfaces prevented the formation of
38
39 aggregates²⁰.
40
41
42

43 Scanning electron microscopy was used to estimate the coverage and dispersion of AuNP on the
44
45 functionalized surfaces. SEM images and graphical estimation of AuNPs density and dispersion
46
47 are shown in Figure 2. The fractional coverage was calculated by dividing the area covered by
48
49 the 2D projection of the spherical AuNPs on the surface by the total area of the surface⁴⁷, results
50
51 are shown in table 2.
52
53

54
55 The coverage and dispersion of the nanoparticles layers were highly dependent on the structure
56
57
58
59
60

1
2
3 of the organic adhesion film. On Au-NH₂ surfaces (Figure 2-d), AuNPs were barely detectable.
4
5 Their absence is ascribable to the application of ultrasounds. Indeed, when the deposition was
6
7 repeated under gentle stirring, SEM images (Supplementary information section, Figure S5)
8
9 showed a small quantity (29 particles/μm²) of gold nanoparticles on the surface, which supports
10
11 the hypothesis of weak interactions between AuNPs and Au-NH₂ surface. Conversely, a
12
13 relatively high density of gold nanoparticles (510±15 x NP/μm²) was observed on Si-NH₂
14
15 substrates (Figure 2-a). This difference observed between Si and Au can be understood by
16
17 considering the difference in amine coverage on the two substrates: while CEA forms a
18
19 monolayer of more or less ordered thiols on gold⁴⁸, APTES condensation on silica-like
20
21 substrates leads to a low amine coverage³⁵. Therefore on Au-NH₂ substrates only amine groups
22
23 are present whereas on Si-NH₂ both silanols (Si-OH) and NH₂ groups are present. Moreover, at
24
25 the acidic pH of AuNPs solutions (pH=5.4), amino groups on Au-NH₂ are mostly positively
26
27 charged, (pK_a (CEA) =8.3⁴⁹), therefore, their interaction with AuNPs can be envisioned mainly
28
29 through electrostatic bonds with negatively charged citrate ligands. Whereas on APTES modified
30
31 surfaces, pK_a=7.6⁵⁰, and though ammonium species dominate, they coexist with silanol groups
32
33 that are negatively charged at this pH (silica PZC=2⁵¹). Silanulates may be involved in AuNP
34
35 interaction with the surface as they can replace citrate ligands and directly interact with gold.
36
37 Therefore, these cooperative interactions on Si-NH₂ would explain the huge difference observed
38
39 with Au-NH₂. Note that despite this cooperative interaction, the coverage observed on Si-NH₂
40
41 layers was the lowest of all the silicon substrates under study (Figure 2 and Table 2).
42
43
44
45
46
47
48
49
50
51
52
53
54
55
56
57
58
59
60

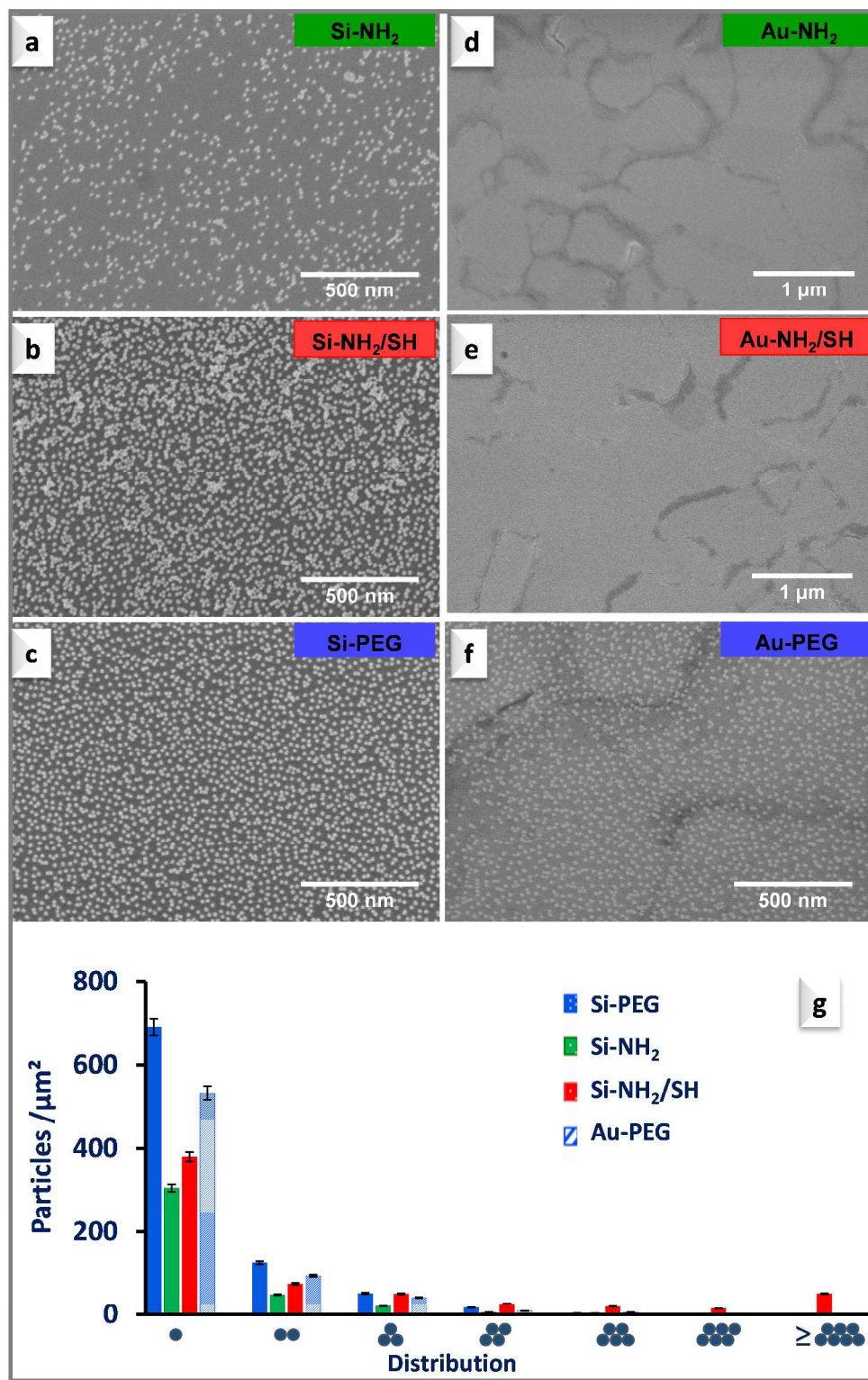


Figure 2 SEM images taken after AuNPs immobilization on the functionalized surfaces (a-f) and the resulting surface coverage (g)

1
2
3 After conjugation of MUA to the amine-terminated surfaces, the Si-NH₂/SH substrates exhibited
4 a higher coverage of AuNPs (Figure 2-b). For Au-NH₂/SH the improvement could not be seen on
5
6 Figure 2-e, but again when the deposition was done without applying ultrasounds (Figure S5,
7
8 Supplementary section) AuNPs coverage was clearly improved compared to on Au-NH₂. This
9
10 result corroborates the efficiency of cooperative interactions towards AuNPs immobilization,
11
12 here through Sulfur/Gold and ammonium/citrate interactions. On Si-NH₂/SH, the fractional
13
14 coverage in AuNPs reached 0.20 (see Table 2). However, the increase in AuNPs coverage on Si-
15
16 NH₂/SH substrates slightly worsen their dispersion, the percentage of isolated particles was
17
18 lowered to 62% and few aggregates were observed (Figure 2-b and g).
19
20
21
22
23

24 The best dispersion of AuNPs and the highest surface coverage were observed for the PEG-
25
26 functionalized substrates, Si-PEG and Au-PEG (Figure 2- c and f). Both systems showed 78% of
27
28 isolated particles and fractional coverage of 0.14 – 0.18 (Table 2). This difference with the
29
30 previous substrates may result from the swelling properties of PEG films that make them capable
31
32 of capturing citrate-stabilized AuNPs²⁷ and trapping them by displacement of loosely bound
33
34 citrate ligands and creation of multidentate interactions between the PEG chains and the Au
35
36 atoms of the AuNPs²⁶. This effect cooperates with the terminal amino group of the PEG chains
37
38 that acts by electrostatic interaction with citrate ligands to stabilize the nanoparticle layers.
39
40 Surprisingly, despite the thick layer of PEG (1.7 nm²⁵), the substrates and/or the organic
41
42 underlayers influence the coverage, as the value is 24% lower on Au-PEG than on Si-PEG.
43
44
45
46
47 Nevertheless, though all the coverage reported in Table 2 may look low, one must keep in mind
48
49 that they in the same range than the data reported in the literature where the deposition and
50
51 washing conditions were less drastic, (0.15 -0.25)^{19, 41, 47}. This limit is determined by the citrate
52
53 ligands co-adsorbed with AuNPs that maintain an electrostatic repulsion between adsorbed
54
55
56
57
58
59
60

1
2
3 citrate-coated AuNPs and prevent the formation of close-packed monolayer^{41, 52-53}.

4
5
6 **Table 2.** AuNPs dispersion and coverage calculated from SEM images

7

Sample	Isolated AuNPs / %	Number of particles / μm^2	Fractional coverage
Si-NH ₂	77	510 \pm 20	0.08
Si-NH ₂ /SH	62	1324 \pm 40	0.20
Si-PEG	78	1186 \pm 40	0.18
Au-PEG	78	905 \pm 30	0.14

8
9
10
11
12
13

14 To summarize this part, offering multiple anchoring points and cooperative interactions
15 improved the coverage and dispersion of gold nanoparticles at the surface of gold and silicon
16 planar substrates. These systems also show a resistance to leaching upon sonication which should
17 make them suitable for further functionalization. The PEG layers provided an excellent
18 dispersion on both substrates (78%). In what follows, we investigate for Si-PEG and Au-PEG
19 substrates the stability of the AuNP layers upon post-functionalization, diclofenac biosensing and
20 under the drastic regeneration conditions.
21
22
23
24
25
26
27
28
29

30
31 **Post-functionalization of gold nanoparticle layers:** The use of the AuNPs-modified platforms
32 for biosensing requires the exchange of the surrounding citrate ligands by reactive functions that
33 will be used to further construct the biosensing layer. Mastering this step is important because the
34 AuNPs layer is mobile and ligand exchange may lead to particle aggregation or leaching from
35 the support⁵⁴⁻⁵⁵. Two reagents were utilized for post-functionalization: CEA and PEG₆₈, both
36 introduce primary amine groups for further anchoring of diclofenac *via* its carboxylic acid
37 function (see molecular structure in **Figure 5**). These post-functionalization treatments were
38 applied to AuNP arrays deposited on PEG-coated silicon and gold substrates. The density and
39 dispersion of AuNPs was then estimated by SEM. Representative images and their mathematical
40 treatment are shown in Figure 3. As expected, post-functionalization modified the AuNP
41 dispersion and coverage. On both substrates, the overall coverage was slightly lowered.
42
43
44
45
46
47
48
49
50
51
52
53
54
55
56
57
58
59
60

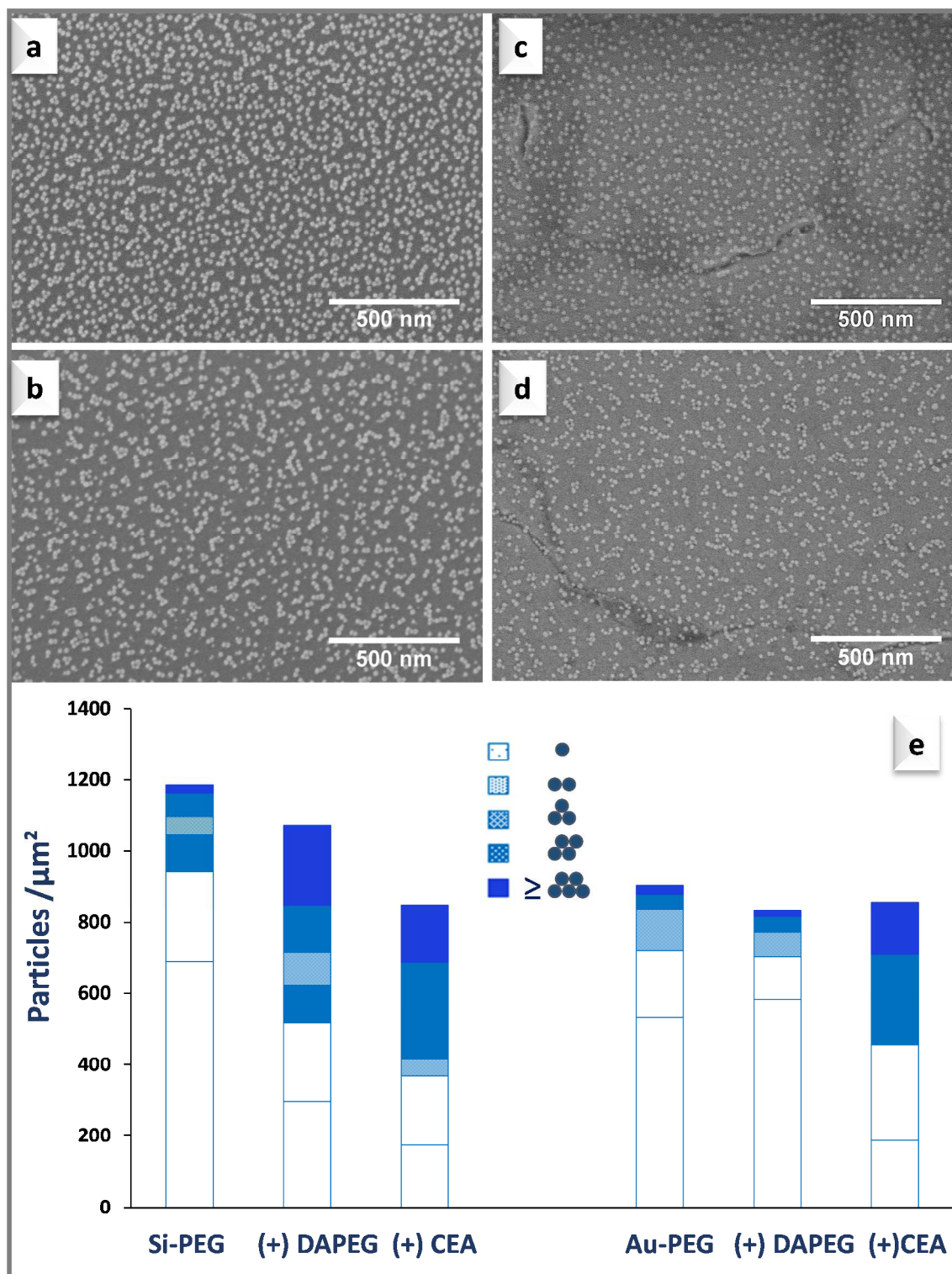


Figure 3 SEM images (a-d) and AuNP densities (e) for Si-PEG-AuNP post-functionalized by CEA (a) or PEG (b) and Au-PEG-AuNP post-functionalized by CEA (c) or PEG (d)

Post-treatment of Si-PEG-AuNP substrates by CEA or DAPEG induced both a significant

1
2
3 desorption of particles (up to 30% with CEA) as well as aggregation. This behavior may be
4 explained by the fact that, since the fractional coverage of AuNP on Si-PEG was higher than 0.15
5 established as the upper limit determined by Grabar et al.⁴¹ for 15-nm diameter citrate-capped
6 AuNPs, the exceeding AuNPs were probably more loosely bound and/or mobile so that further
7 treatment with a weak ligand like DAPEG favored aggregation whereas further treatment with a
8 stronger adsorbate like CEA led to both aggregation and desorption. Similar desorption was
9 previously reported on APTES-coated silicon upon treatment with CEA and explained by the
10 positive charge of nanoparticles upon citrate ions replacement by CEA molecules that led to
11 repulsion from the positively charged APTES-coated surface^{52,55}. Conversely, post-
12 functionalization of Au-PEG-AuNP by CEA or DAPEG did only marginally affect the overall
13 particle density. This is in line with the fractional coverage being lower than 0.15, and therefore
14 the probable absence of loosely bound particles on this surface. Furthermore, particle
15 aggregation was only induced by CEA. In this situation, repulsion due to negative charges of
16 citrates was no longer effective and aggregates formed⁵³. On the whole, post-treatment on Au-
17 PEG-AuNP by DAPEG allowed maintaining a high density of NP as well as a good dispersion.
18 The nanostructured Si-PEG-AuNP and Au-PEG-AuNP substrates post-functionalized with
19 DAPEG were further selected to build up a piezoelectric immunosensor for the anti-
20 inflammatory drug diclofenac.

21
22
23
24
25
26
27
28
29
30
31
32
33
34
35
36
37
38
39
40
41
42
43
44
45
46 **Anti-diclofenac antibody recognition, specificity and reversibility:** Diclofenac was covalently
47 bound through its carboxylic acid function to the PEG amino groups of the nanostructured gold
48 and silicon sensors and recognition of anti-diclofenac antibody was investigated by QCM-D as
49 depicted in Figure 4. QCM was also used to assess the specificity of recognition towards non
50 specific anti-mouse IgG (Supplementary section, Figure S6) as well as the reversibility of the
51
52
53
54
55
56
57
58
59
60

haptent / antibody interaction (Supplementary section, Figure S7). In addition, to determine whether nanostructuring benefits to target recognition, the same experiment was run on flat silicon and gold substrates modified by GOPTS-PEG and MUA-PEG, respectively (Figure 4).

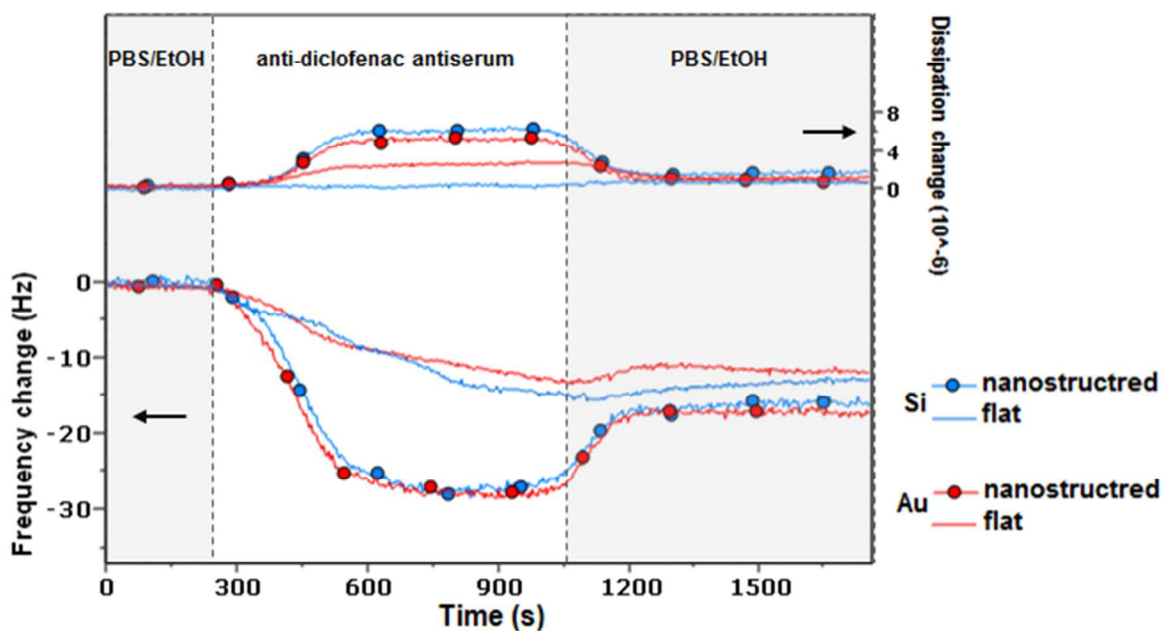


Figure 4 Frequency and dissipation shifts monitored during capture of anti-diclofenac antibody and washing with carrier buffer with the 4 different immunosensors

Injection of non-specific antibody had no influence on the resonance frequency (Figure S6). Conversely, injection of anti-diclofenac antibody resulted in an immediate decrease of the resonance frequency of the 4 sensors confirming the recognition of the specific anti-diclofenac antibody by the capture layer comprising diclofenac (Figure 4). The magnitude of the shift (ΔF) as well as the rate of frequency change $d\Delta F/dt$ were highly dependent on the nature of the sensing layer. On all systems, applying a regeneration buffer (pH=2) led to the release of the captured antibodies and return to the initial frequency (Figure S7).

We also analyzed the AuNPs layers by SEM to establish the possible effect of

immunorecognition and regeneration on their dispersion and coverage. The SEM images in Figure 5 show that the gold nanoparticles layer was remarkably stable after the biorecognition step and even after the drastic regeneration conditions at acidic pH. No change was recorded upon anti-diclofenac binding to the surface. Upon regeneration, the drastic conditions applied led to a decrease in nanoparticle dispersion, yet, only small aggregates were formed and less than 15% of AuNP formed aggregates larger than 4 units. The regeneration process needs to be optimized to further limit its impact on AuNP dispersion.

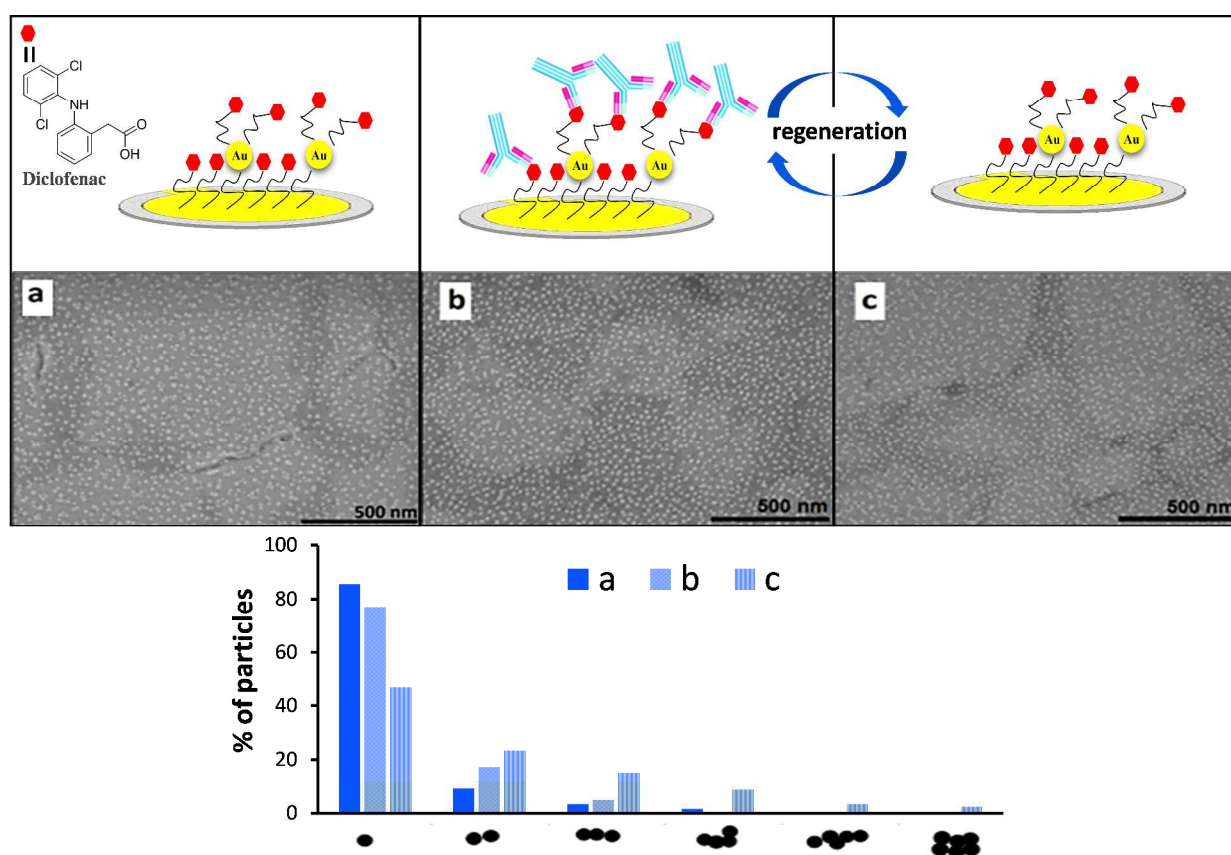


Figure 5 Reversible immunorecognition scheme and SEM images and data of Au-PEG gold nanoparticles platforms post-functionalized with PEG₆₈ at the successive stages of the immunoreaction

Mass uptakes Δm were calculated from the frequency shifts by applying the Sauerbrey equation

1
2
3 since dissipation shifts were lower than 1×10^{-6} during antibody capture (Table 3). The QCM
4
5 responses in terms of ΔF and $d\Delta F/dt$ were significantly larger for the 2 nanostructured sensor
6
7 chips in agreement with the increase of specific surface brought by the layer of AuNPs. Clearly,
8
9 the two flat sensors had lower antibody binding capacity than the nanostructured ones. Before
10
11 washing with buffer, the increase was over 120% for both substrates, i.e. more than 6 times
12
13 higher than on flat surfaces. After washing, the input of nanostructuring was still important, 32
14
15 and 48% for silicon and gold, respectively. The origin of this enhancement may be geometrical
16
17 as the nanostructured sensors display a higher specific area than the flat ones. Knowing the
18
19 surface coverage in AuNPs and their mean size, the increase of accessible surface area can be
20
21 readily estimated. We have done these calculations depending on the exposed height of AuNPs
22
23 (i.e. how the AuNPs are actually embedded in the organic film). The increase in area ranged from
24
25 17 to 33% for the Si sensor (with 1073 particles/ μm^2) and from 13 to 26% for the Au sensor
26
27 (with 833 particles / μm^2). Alternatively, the surface topology of nanostructured sensors may also
28
29 favor the accessibility of the immobilized diclofenac ligand towards its antibody further
30
31 enhancing the geometric benefit of nanostructuring.
32
33
34
35
36
37
38
39
40

41 **Table 3** QCM data for flat and AuNPs nanostructured surfaces

	Gold		Silicon	
	Flat	Nanostructured	Flat	Nanostructured
$-\Delta F_5$ (Hz)	11.8	17.5 ± 1	12.5	16.5 ± 0.5
$\Delta m/A$ (ng/cm ²)	208	310 ± 18	222	293 ± 9
$\Gamma(\text{exp})$ (pmol.cm ⁻²)*	1.4	2	1.5	1.95
Increase (%) before washing	---	128	---	124
Increase after washing (%)	---	48	---	32
$-d\Delta F/dt$ (Hz.s ⁻¹)	0.016	0.077	0.019	0.088

42
43
44
45
46
47
48
49
50
51
52
53
54
55 Furthermore, the nanostructured surfaces on a silicon or gold substrates gave very similar
56
57 responses in QCM. The amount of anti-diclofenac antibodies recognizing the target differs little
58
59
60

1
2
3 despite a difference in the total density of AuNPs greater than 20% for silicon substrates. This
4
5 result corroborates the assumption that increasing the surface area is the one and only reason of
6
7 the improved performances of nanostructured immunosensors and abounds and towards a greater
8
9 contribution granted by the new surface topology and the increased accessibility of the target.
10
11 This result thus also proves that, at this stage, the influence of the substrate is limited which
12
13 paves the way for a generalization of this surface chemistry to other substrates by expecting the
14
15 same performances.
16
17
18
19

20
21 To conclude this part, AuNPs layers led to a significant enhancement in the biosensor sensitivity.
22
23 This enhancement presages a higher sensitivity in the competitive detection of diclofenac on
24
25 these systems. More importantly, despite the biorecognition and the drastic regeneration
26
27 conditions, gold nanoparticle layers were stable and reliable, which paves the way for their use
28
29 as nanostructured platforms for various applications.
30
31
32
33

34 35 CONCLUSION

36
37 Different surface chemistries were devised to generate layers of gold nanoparticles (AuNPs) on
38
39 gold and silicon planar substrates. Adhesion layers either included alkyl chains or poly(ethylene
40
41 glycol) (PEG) and were terminated by amines or mixed amine and thiol groups. The assembly of
42
43 gold nanoparticles on the functionalized substrates was studied in depth by Scanning Electron
44
45 Microscopy. The highest coverage and dispersion were reached when gold nanoparticles were
46
47 deposited on adhesion layers offering multiple anchoring points and cooperative interactions.
48
49 These systems showed a resistance to leaching upon sonication which made them suitable for
50
51 further functionalization. Adhesion layers including PEG motifs provided an excellent coverage
52
53 and the best dispersion on both Si and Au substrates (78%). These layers were post-
54
55
56
57
58
59
60

1
2
3 functionalized using either PEG-diamine or cysteamine to exchange the surrounding citrate
4
5 ligands by reactive functions that will be used to further bind the bioreceptors. This step slightly
6
7 decreased the coverage in gold nanoparticles, particularly on silicon substrates, but the use of
8
9 PEG-diamine better preserved the dispersion of gold nanoparticles. The resulting layers were
10
11 successfully used to build up a piezoelectric immunosensor for the anti-inflammatory drug
12
13 diclofenac. They were sensitive and specific to diclofenac antibody. Compared to planar
14
15 surfaces, they showed a significant enhancement in the biosensor sensitivity, up to 6 times the
16
17 signal recorded for planar substrates. More importantly, despite the biorecognition and the drastic
18
19 regeneration conditions, QCM sensors covered with gold nanoparticle layers were stable and
20
21 reusable with a preserved coverage and dispersion, which paves the way for their use as
22
23 nanostructured platforms for various applications.
24
25
26
27
28
29

30 SUPPORTING INFORMATION

31
32
33 Gold nanoparticles characterizations. IR characterization of functionalized surfaces. Gold
34
35 nanoparticles deposition. QCM data.
36
37
38

39 ACKNOWLEDGEMENTS

40
41
42 We would like to thank the DIM Analytics and Region Ile-de-France for M. Ben Haddada PhD
43
44 scholarship. This work was also co-financially supported by ANR (Agence Nationale de la
45
46 Recherche) and DFG (Deutsche Forschungsgemeinschaft), ANR-DFG program, project
47
48 NArBioS, Grant no: ANR-11-INTB-1013.
49
50
51
52
53
54
55
56
57
58
59
60

REFERENCES

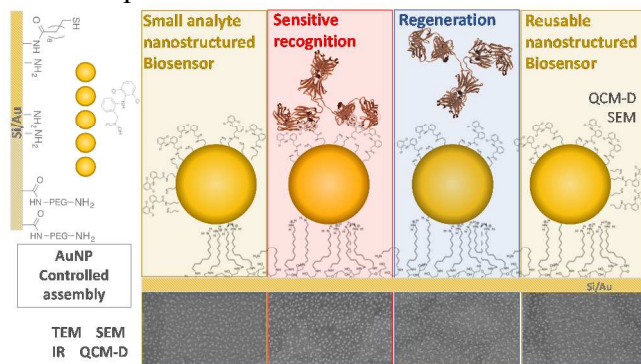
1. Saha, K.; Agasti, S. S.; Kim, C.; Li, X. N.; Rotello, V. M., Gold Nanoparticles in Chemical and Biological Sensing. *Chem. Rev.* **2012**, *112*, 2739-2779.
2. Nath, N.; Chilkoti, A., Label-Free Biosensing by Surface Plasmon Resonance of Nanoparticles on Glass: Optimization of Nanoparticle Size. *Anal. Chem.* **2004**, *76*, 5370-5378.
3. Sepulveda, B.; Angelome, P. C.; Lechuga, L. M.; Liz-Marzan, L. M., LSPR-Based Nanobiosensors. *Nano Today* **2009**, *4*, 244-251.
4. Stewart, M. E.; Anderton, C. R.; Thompson, L. B.; Maria, J.; Gray, S. K.; Rogers, J. A.; Nuzzo, R. G., Nanostructured Plasmonic Sensors. *Chem. Rev.* **2008**, *108*, 494-521.
5. Fan, M. K.; Andrade, G. F. S.; Brolo, A. G., A Review on the Fabrication of Substrates for Surface Enhanced Raman Spectroscopy and Their Applications in Analytical Chemistry. *Anal. Chim. Acta* **2011**, *693*, 7-25.
6. Felicia, T.; Monica, B.; Lucian, B.; Simion, A., Controlling Gold Nanoparticle Assemblies for Efficient Surface-Enhanced Raman Scattering and Localized Surface Plasmon Resonance Sensors. *Nanotechnology* **2007**, *18*, 255702.
7. Fonseca, R. A. S.; Ramos-Jesus, J.; Kubota, L. T.; Dutra, R. F., A Nanostructured Piezoelectric Immunosensor for Detection of Human Cardiac Troponin T. *Sensors* **2011**, *11*, 10785-10797.
8. Kong, L.-J.; Pan, M.-F.; Fang, G.-Z.; He, X.-l.; Yang, Y.-k.; Dai, J.; Wang, S., Molecularly Imprinted Quartz Crystal Microbalance Sensor Based on Poly(O-Aminothiophenol) Membrane and Au Nanoparticles for Ractopamine Determination. *Biosens. Bioelectron.* **2014**, *51*, 286-292.
9. Cai, H.; Xu, C.; He, P.; Fang, Y., Colloid Au-Enhanced DNA Immobilization for the Electrochemical Detection of Sequence-Specific DNA. *J. Electroanal. Chem.* **2001**, *510*, 78-85.
10. Liu, T.; Tang, J. a.; Jiang, L., The Enhancement Effect of Gold Nanoparticles as a Surface Modifier on DNA Sensor Sensitivity. *Biochem. Biophys. Res. Commun.* **2004**, *313*, 3-7.
11. Liu, S.-f.; Li, J.-R.; Jiang, L., Surface Modification of Platinum Quartz Crystal Microbalance by Controlled Electroless Deposition of Gold Nanoparticles and Its Enhancing Effect on the Hs-DNA Immobilization. *Colloids Surf. Physicochem. Eng. Aspects* **2005**, *257-258*, 57-62.
12. Chu, P.-T.; Lin, C.-S.; Chen, W.-J.; Chen, C.-F.; Wen, H.-W., Detection of Gliadin in Foods Using a Quartz Crystal Microbalance Biosensor That Incorporates Gold Nanoparticles. *J. Agric. Food. Chem.* **2012**, *60*, 6483-6492.
13. Vidal, J. C.; Duato, P.; Bonel, L.; Castillo, J. R., Use of Polyclonal Antibodies to Ochratoxin a with a Quartz-Crystal Microbalance for Developing Real-Time Mycotoxin Piezoelectric Immunosensors. *Anal. Bioanal. Chem.* **2009**, *394*, 575-582.
14. Wang, H.; Liu, Y. L.; Yang, Y. H.; Deng, T.; Shen, G. L.; Yu, R. Q., A Protein a-Based Orientation-Controlled Immobilization Strategy for Antibodies Using Nanometer-Sized Gold Particles and Plasma-Polymerized Film. *Anal. Biochem.* **2004**, *324*, 219-226.
15. Wang, H.; Wu, J.; Li, J.; Ding, Y.; Shen, G.; Yu, R., Nanogold Particle-Enhanced Oriented Adsorption of Antibody Fragments for Immunosensing Platforms. *Biosens. Bioelectron.* **2005**, *20*, 2210-2217.
16. Makaraviciute, A.; Ruzgas, T.; Ramanavicius, A.; Ramanaviciene, A., Antibody Fragment Immobilization on Planar Gold and Gold Nanoparticle Modified Quartz Crystal Microbalance with Dissipation Sensor Surfaces for Immunosensor Applications. *Anal. Meth.* **2014**, *6*, 2134-2140.

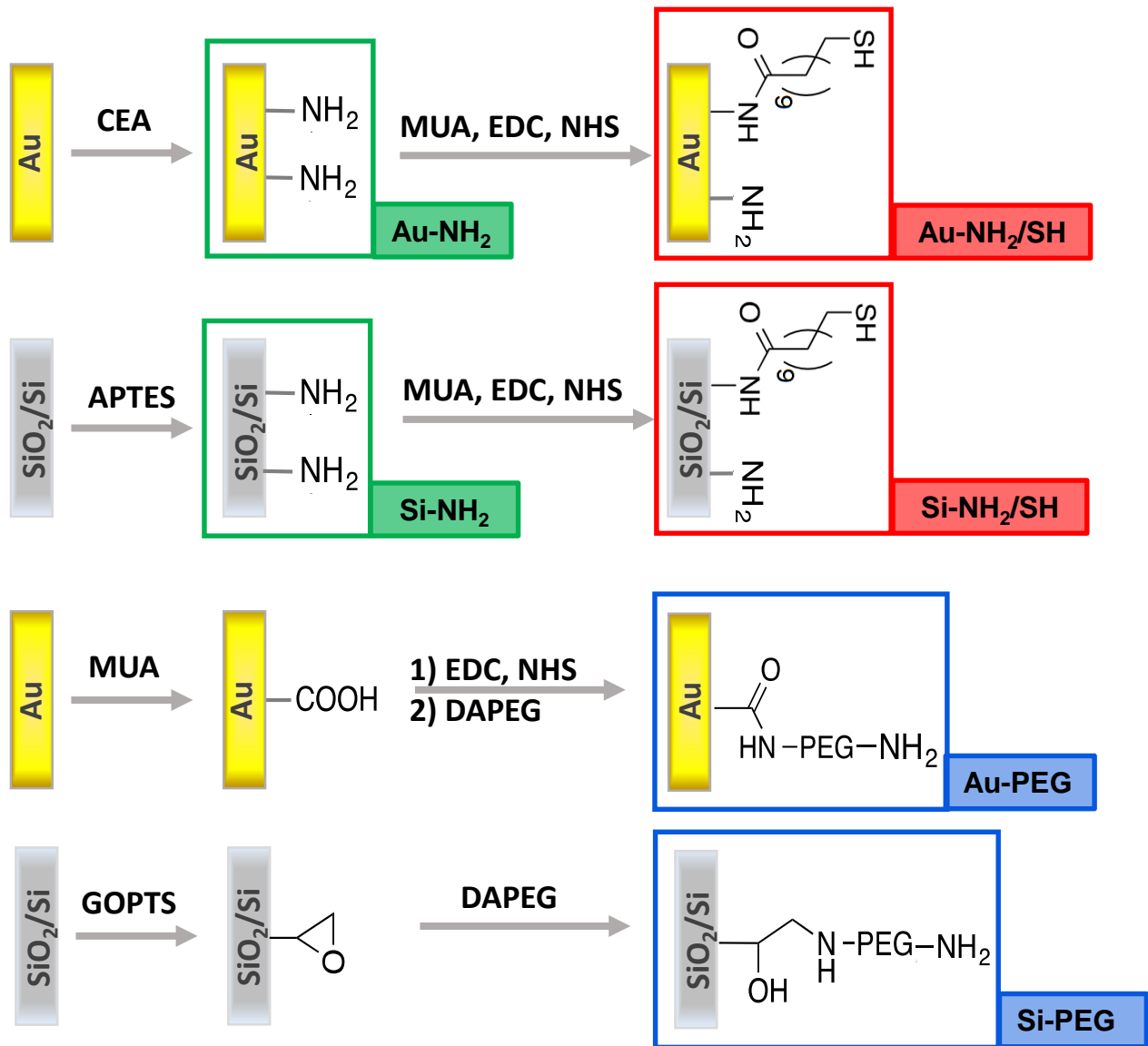
17. Turkevich, J.; Stevenson, P. C.; Hillier, J., A Study of the Nucleation and Growth Processes in the Synthesis of Colloidal Gold. *Farad. Disc.* **1951**, 55-&.
18. Morel, A.-L.; Boujday, S.; Méthivier, C.; Krafft, J.-M.; Pradier, C.-M., Biosensors Elaborated on Gold Nanoparticles, a PM-IRRAS Characterisation of the IgG Binding Efficiency. *Talanta* **2011**, 85, 35-42.
19. Morel, A.-L.; Volmant, R.-M.; Méthivier, C.; Krafft, J.-M.; Boujday, S.; Pradier, C.-M., Optimized Immobilization of Gold Nanoparticles on Planar Surfaces through Alkyldithiols and Their Use to Build 3D Biosensors. *Colloids Surf., B* **2010**, 81, 304-312.
20. Ben Haddada, M., Optimizing the Immobilization of Gold Nanoparticles on Functionalized Silicon Surfaces: Amine- Vs Thiol-Terminated Silane. *Gold Bulletin* **2013**, 1-7.
21. Aissaoui, N.; Bergaoui, L.; Landoulsi, J.; Lambert, J.-F.; Boujday, S., Silane Layers on Silicon Surfaces: Mechanism of Interaction, Stability, and Influence on Protein Adsorption. *Langmuir* **2012**, 28, 656-665.
22. Christau, S.; Moller, T.; Yenice, Z.; Genzer, J.; von Klitzing, R., Brush/Gold Nanoparticle Hybrids: Effect of Grafting Density on the Particle Uptake and Distribution within Weak Polyelectrolyte Brushes. *Langmuir* **2014**, 30, 13033-13041.
23. Christau, S.; Thurandt, S.; Yenice, Z.; von Klitzing, R., Stimuli-Responsive Polyelectrolyte Brushes as a Matrix for the Attachment of Gold Nanoparticles: The Effect of Brush Thickness on Particle Distribution. *Polymers* **2014**, 6, 1877-1896.
24. Mehne, J.; Markovic, G.; Pröll, F.; Schweizer, N.; Zorn, S.; Schreiber, F.; Gauglitz, G., Characterisation of Morphology of Self-Assembled Peg Monolayers: A Comparison of Mixed and Pure Coatings Optimised for Biosensor Applications. *Anal. Bioanal. Chem.* **2008**, 391, 1783-1791.
25. Huebner, M.; Ben Haddada, M.; Methivier, C.; Niessner, R.; Knopp, D.; Boujday, S., Layer-by-Layer Generation of Peg-Based Regenerable Immunosensing Surfaces for Small-Sized Analytes. *Biosens. Bioelectron.* **2015**, 67, 334-341.
26. Diamanti, S.; Arifuzzaman, S.; Genzer, J.; Vaia, R. A., Tuning Gold Nanoparticle–Poly(2-Hydroxyethyl Methacrylate) Brush Interactions: From Reversible Swelling to Capture and Release. *ACS Nano* **2009**, 3, 807-818.
27. Meyerbröker, N.; Kriesche, T.; Zharnikov, M., Novel Ultrathin Poly(Ethylene Glycol) Films as Flexible Platform for Biological Applications and Plasmonics. *ACS Appl. Mater. Interfaces* **2013**, 5, 2641-2649.
28. Daniel, M. C.; Astruc, D., Gold Nanoparticles: Assembly, Supramolecular Chemistry, Quantum-Size-Related Properties, and Applications toward Biology, Catalysis, and Nanotechnology. *Chem. Rev.* **2004**, 104, 293-346.
29. Brust, M.; Fink, J.; Bethell, D.; Schiffrin, D. J.; Kiely, C., Synthesis and Reactions of Functionalized Gold Nanoparticles. *Chem. Commun.* **1995**, 1655-1656.
30. Pena-Pereira, F.; Duarte, R. M. B. O.; Duarte, A. C., Immobilization Strategies and Analytical Applications for Metallic and Metal-Oxide Nanomaterials on Surfaces. *TrAC, Trends Anal. Chem.* **2012**, 40, 90-105.
31. Lundgren, A.; Hulander, M.; Brorsson, J.; Hermansson, M.; Elwing, H.; Andersson, O.; Liedberg, B.; Berglin, M., Gold-Nanoparticle-Assisted Self-Assembly of Chemical Gradients with Tunable Sub-50 Nm Molecular Domains. *Part. Part. Syst. Charact.* **2014**, 31, 209-218.
32. Deng, A. P.; Himmelsbach, M.; Zhu, Q. Z.; Frey, S.; Sengl, M.; Buchberger, W.; Niessner, R.; Knopp, D., Residue Analysis of the Pharmaceutical Diclofenac in Different Water Types Using Elisa and Gc-Ms. *Environ. Sci. Technol.* **2003**, 37, 3422–3429.

- 1
2
3 33. Huebner, M.; Weber, E.; Niessner, R.; Boujday, S.; Knopp, D., Rapid Analysis of
4 Diclofenac in Freshwater and Wastewater by a Monoclonal Antibody-Based Highly Sensitive
5 Elisa. *Anal. Bioanal. Chem.* **2015**, *407*, 8873-8882.
- 6
7 34. Cras, J. J.; Rowe-Taitt, C. A.; Nivens, D. A.; Ligler, F. S., Comparison of Chemical
8 Cleaning Methods of Glass in Preparation for Silanization. *Biosens. Bioelectron.* **1999**, *14*, 683-
9 688.
- 10 35. Aissaoui, N.; Bergaoui, L.; Landoulsi, J.; Lambert, J. F.; Boujday, S., Silane Layers on
11 Silicon Surfaces: Mechanism of Interaction, Stability, and Influence on Protein Adsorption.
12 *Langmuir* **2012**, *28*, 656-65.
- 13 36. Slot, J. W.; Geuze, H. J., A Method to Prepare Isodisperse Colloidal Gold Sols in the Size
14 Range 3–17 Nm. *Ultramicroscopy* **1984**, *15*, 383.
- 15 37. Boujday, S.; Gu, C.; Girardot, M.; Salmain, M.; Pradier, C.-M., Surface Ir Applied to
16 Rapid and Direct Immunosensing of Environmental Pollutants. *Talanta* **2009**, *78*, 165-170.
- 17 38. Sauerbrey, G., The Use of Quartz Oscillators for Weighing Thin Layers and for
18 Microweighing. *Z. Phys.* **1959**, *155*, 206-22.
- 19 39. Seitz, O.; Chehimi, M. M.; Cabet-Deliry, E.; Truong, S.; Felidj, N.; Perruchot, C.;
20 Greaves, S. J.; Watts, J. F., Preparation and Characterisation of Gold Nanoparticle Assemblies on
21 Silanised Glass Plates. *Colloids Surf., A* **2003**, *218*, 225-239.
- 22 40. Link, S.; El-Sayed, M. A., Size and Temperature Dependence of the Plasmon Absorption
23 of Colloidal Gold Nanoparticles. *J. Phys. Chem. B* **1999**, *103*, 4212-4217.
- 24 41. Grabar, K. C.; Freeman, R. G.; Hommer, M. B.; Natan, M. J., Preparation and
25 Characterization of Au Colloid Monolayers. *Anal. Chem.* **1995**, *67*, 735-743.
- 26 42. Onses, M. S.; Nealey, P. F., Tunable Assembly of Gold Nanoparticles on Nanopatterned
27 Poly(Ethylene Glycol) Brushes. *Small* **2013**, *9*, 4168-4174.
- 28 43. Kanan, S. M.; Tze, W. T. Y.; Tripp, C. P., Method to Double the Surface Concentration
29 and Control the Orientation of Adsorbed (3-Aminopropyl)Dimethylethoxysilane on Silica
30 Powders and Glass Slides. *Langmuir* **2002**, *18*, 6623-6627.
- 31 44. Vericat, C.; Vela, M. E.; Salvarezza, R. C., Self-Assembled Monolayers of Alkanethiols
32 on Au(111): Surface Structures, Defects and Dynamics. *PCCP* **2005**, *7*, 3258-3268.
- 33 45. Vallee, A.; Humblot, V.; Al Housseiny, R.; Boujday, S.; Pradier, C.-M., Bsa Adsorption on
34 Aliphatic and Aromatic Acid Sams: Investigating the Effect of Residual Surface Charge and
35 Sublayer Nature. *Colloids Surf., B* **2013**, *109*, 136-142.
- 36 46. Harder, P.; Grunze, M.; Dahint, R.; Whitesides, G. M.; Laibinis, P. E., Molecular
37 Conformation in Oligo(Ethylene Glycol)-Terminated Self-Assembled Monolayers on Gold and
38 Silver Surfaces Determines Their Ability to Resist Protein Adsorption. *J. Phys. Chem. B* **1998**,
39 *102*, 426-436.
- 40 47. Nath, N.; Chilkoti, A., Label-Free Biosensing by Surface Plasmon Resonance of
41 Nanoparticles on Glass: Optimization of Nanoparticle Size. *Anal. Chem.* **2004**, *76*, 5370-5378.
- 42 48. Bedford, E.; Humblot, V.; Methivier, C.; Pradier, C.-M.; Gu, F.; Tielens, F.; Boujday, S.,
43 An Experimental and Theoretical Approach to Investigate the Effect of Chain Length on
44 Aminothiols Adsorption and Assembly on Gold. *Chem. Eur. J.* **2015**, *21*, 14555-14561.
- 45 49. Riauba, L.; Niaura, G.; Eicher-Lorka, O.; Butkus, E., A Study of Cysteamine Ionization
46 in Solution by Raman Spectroscopy and Theoretical Modeling. *J. Phys. Chem. A* **2006**, *110*,
47 13394-13404.
- 48 50. Bhat, R. R.; Genzer, J., Tuning the Number Density of Nanoparticles by Multivariant
49 Tailoring of Attachment Points on Flat Substrates. *Nanotechnology* **2007**, *18*.
- 50
51
52
53
54
55
56
57
58
59
60

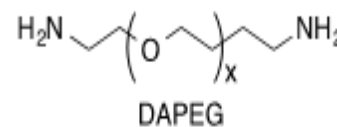
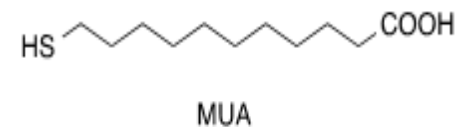
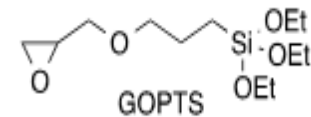
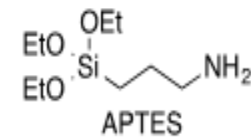
- 1
2
3 51. Iler, R. K., *The Chemistry of Silica*; Wiley-Interscience: New York, 1979.
4 52. Enders, D.; Nagao, T.; Pucci, A.; Nakayama, T., Reversible Adsorption of Au
5 Nanoparticles on SiO₂/Si: An in Situ Atr-Ir Study. *Surf. Sci.* **2006**, *600*, L71-L75.
6 53. Sato, T.; Ahmed, H.; Brown, D.; Johnson, B. F. G., Single Electron Transistor Using a
7 Molecularly Linked Gold Colloidal Particle Chain. *J. Appl. Phys.* **1997**, *82*, 696-701.
8 54. Sato, T.; Brown, D.; Johnson, B. F. G., Nucleation and Growth of Nano-Gold Colloidal
9 Lattices. *Chem. Commun.* **1997**, 1007-1008.
10 55. Enders, D.; Nagao, T.; Nakayama, T.; Aono, M., In Situ Surface-Enhanced Infrared
11 Absorption Spectroscopy for the Analysis of the Adsorption and Desorption Process of Au
12 Nanoparticles on the SiO₂/Si Surface. *Langmuir* **2007**, *23*, 6119-6125.
13
14
15
16
17
18
19
20
21
22
23
24
25
26
27
28
29
30
31
32
33
34
35
36
37
38
39
40
41
42
43
44
45
46
47
48
49
50
51
52
53
54
55
56
57
58
59
60

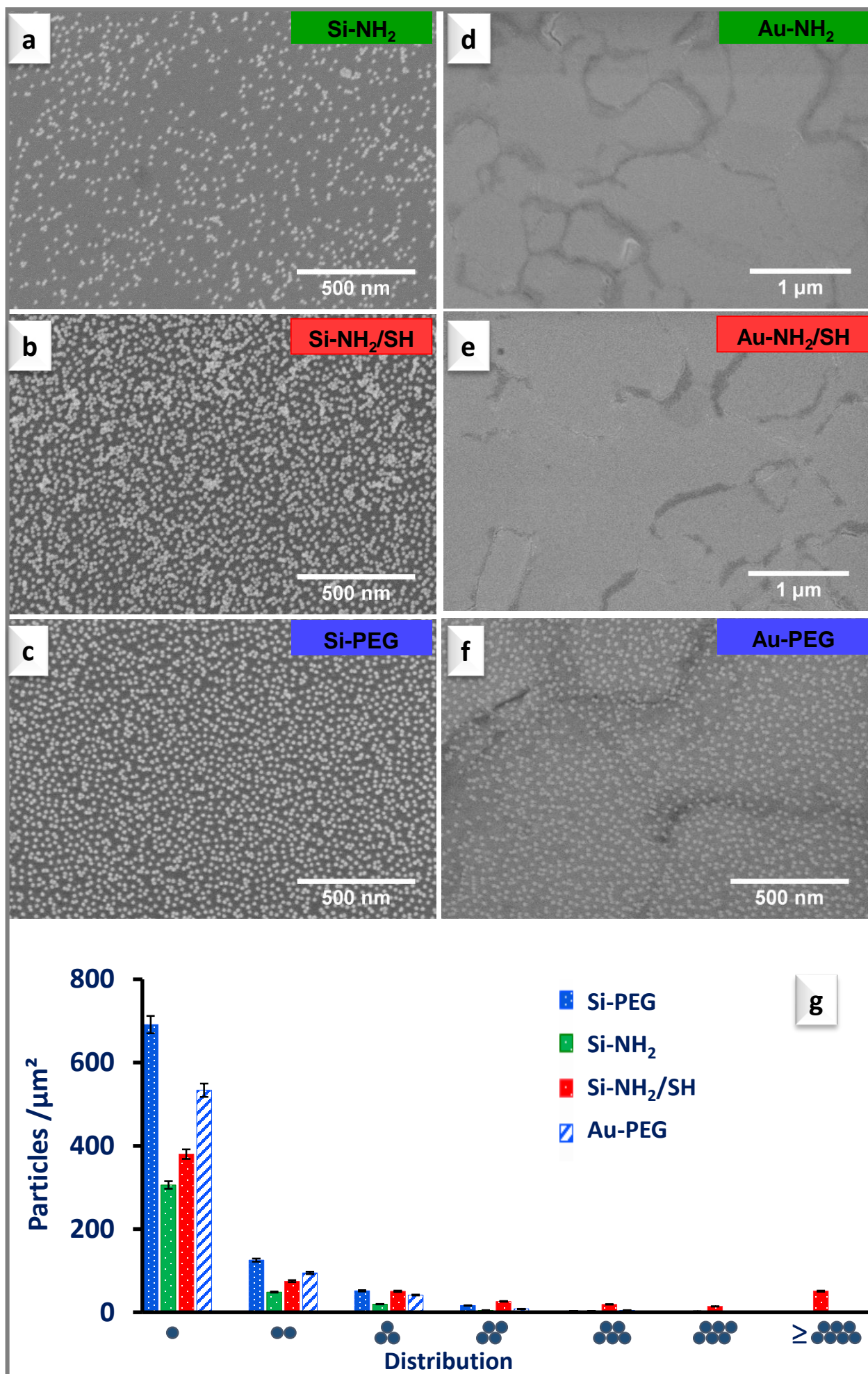
TOC Graphic

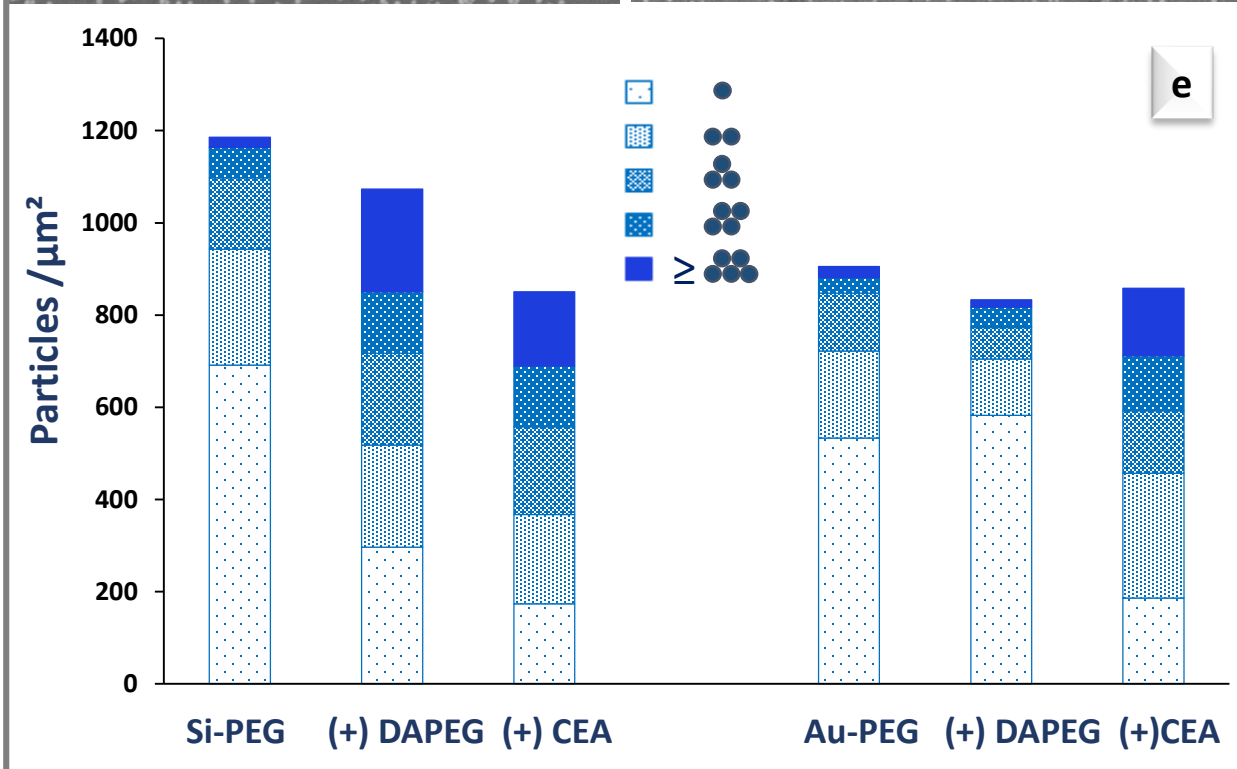
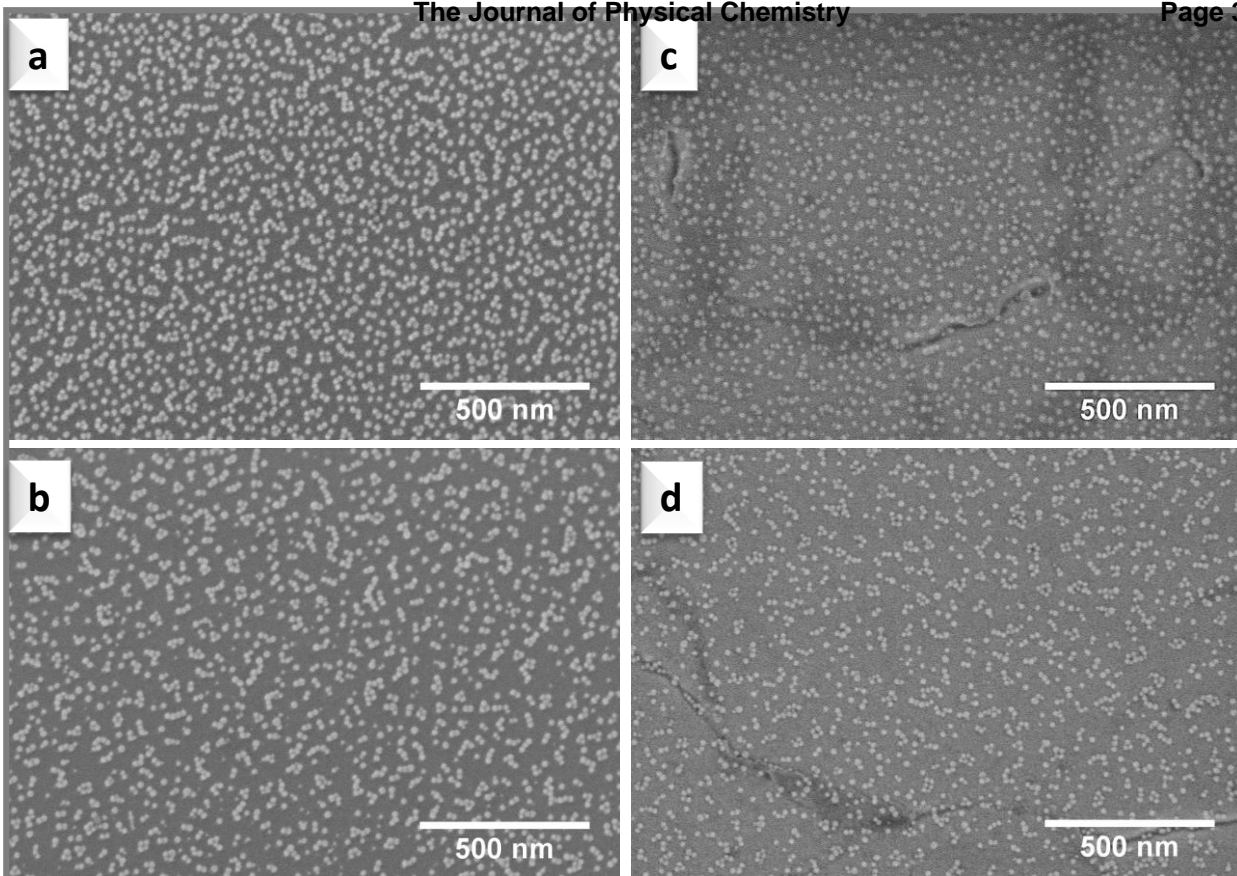


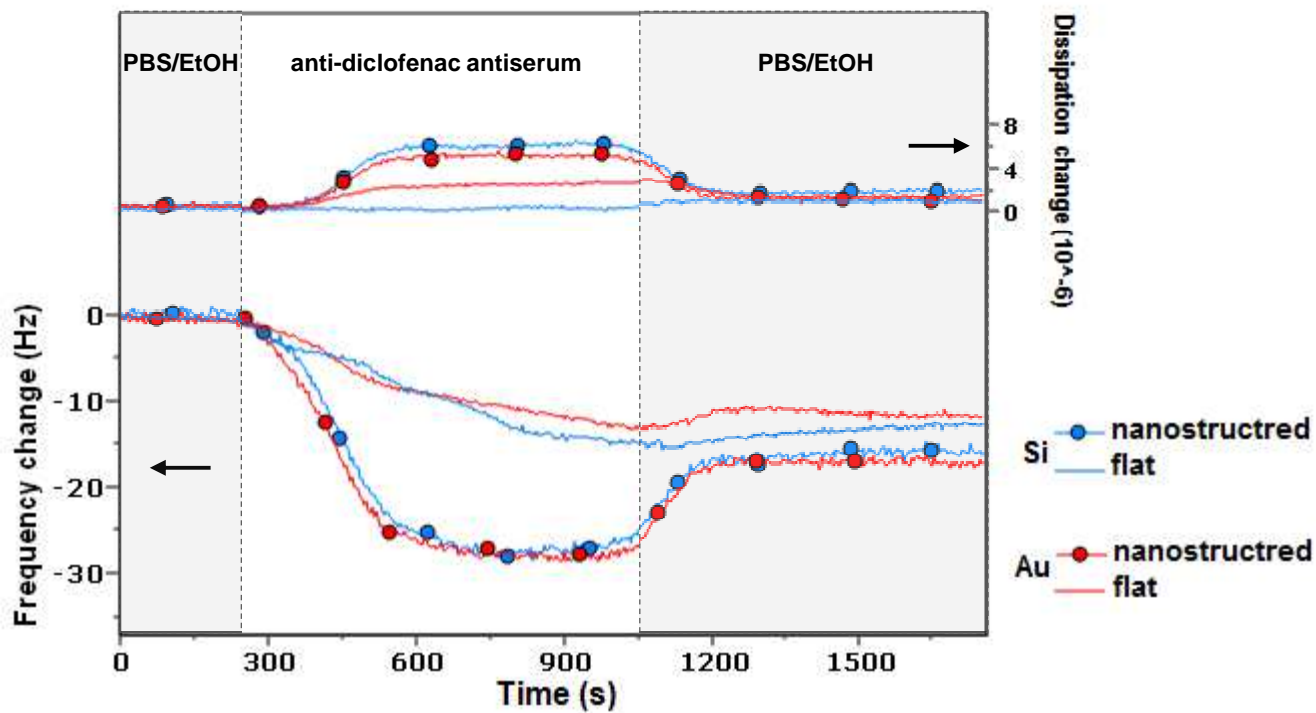


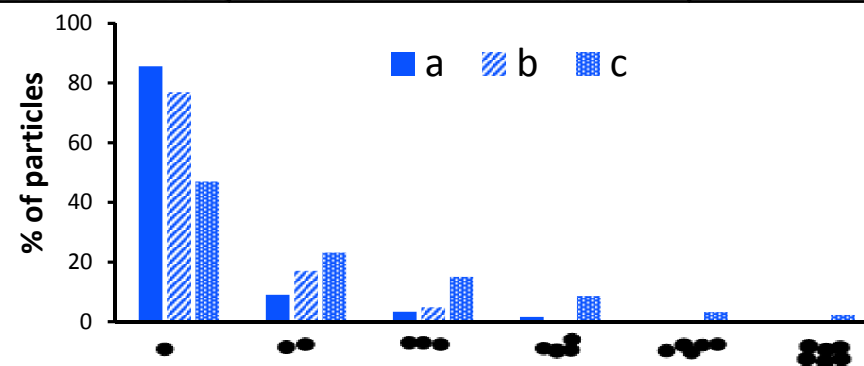
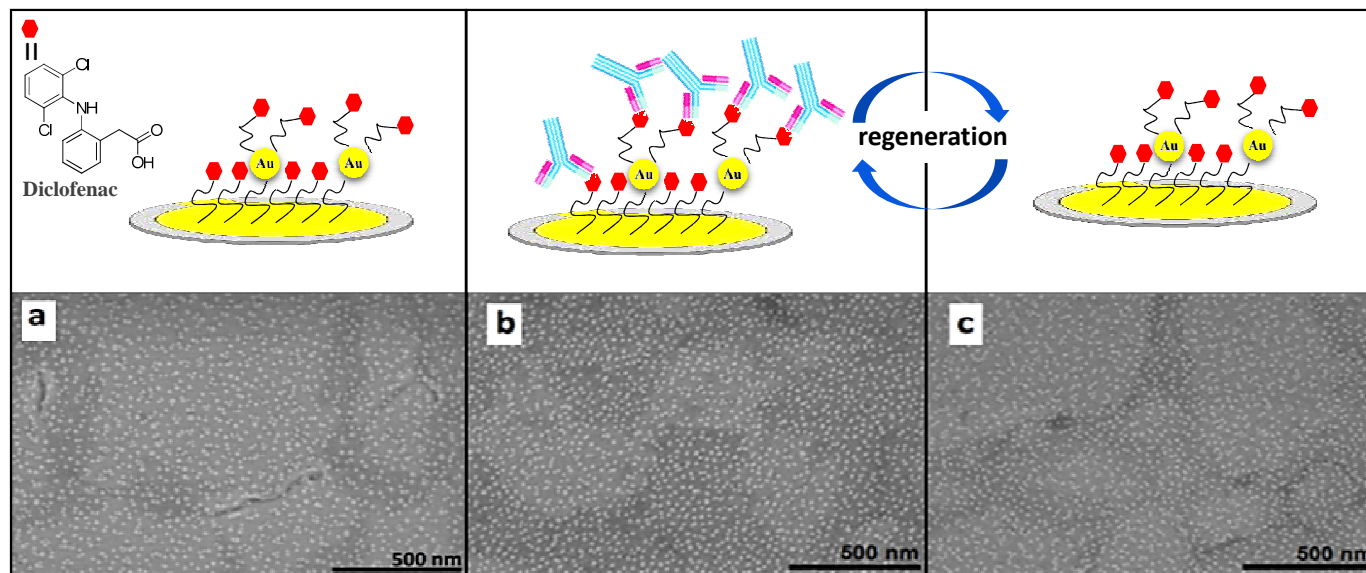
Reagents



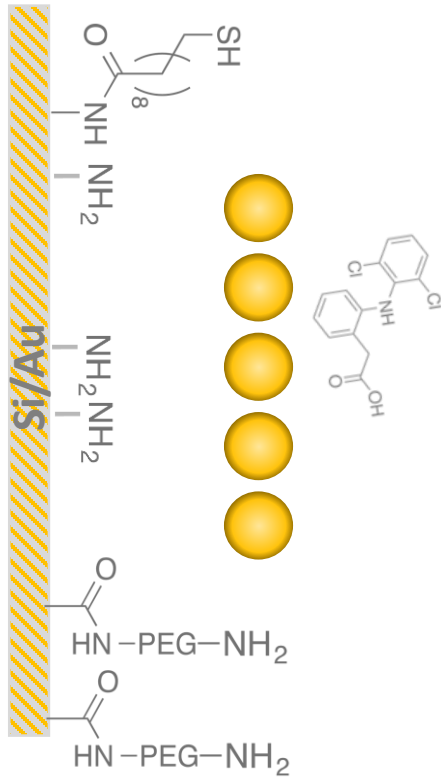






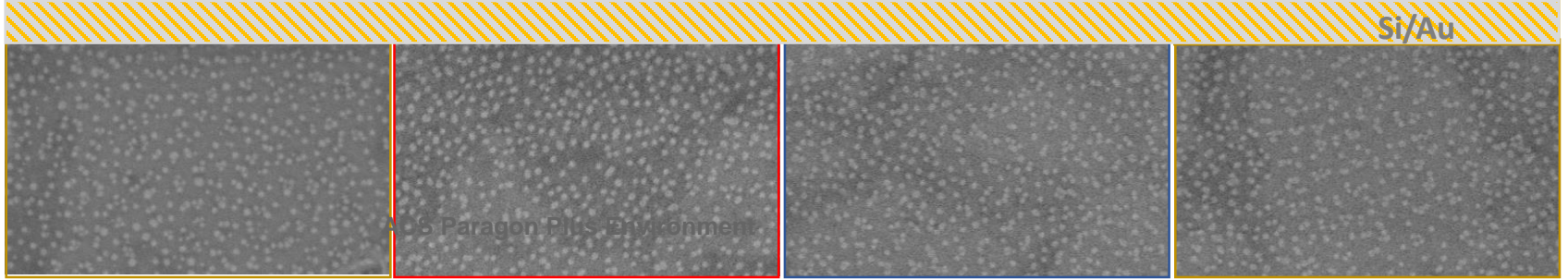
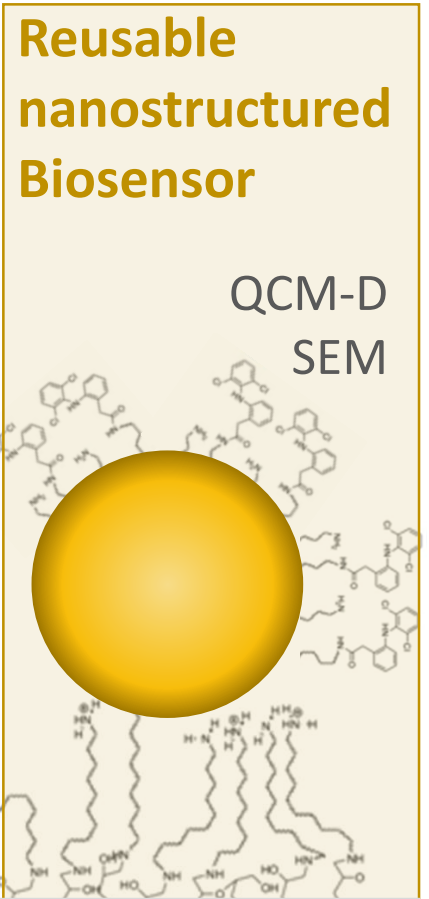
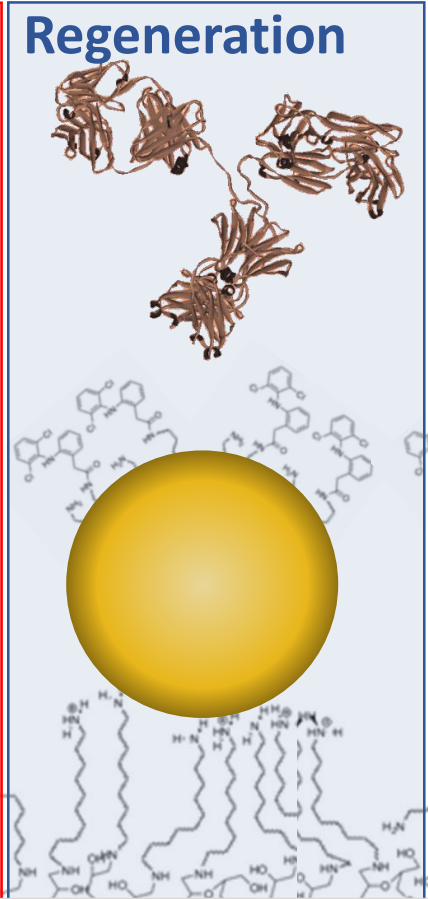
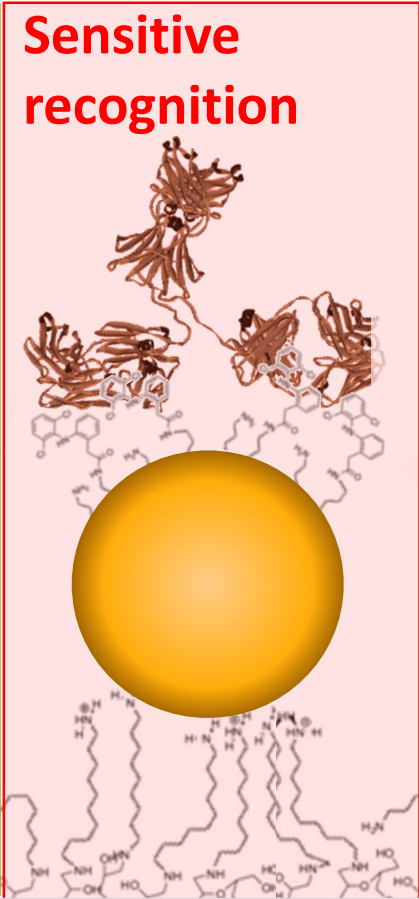
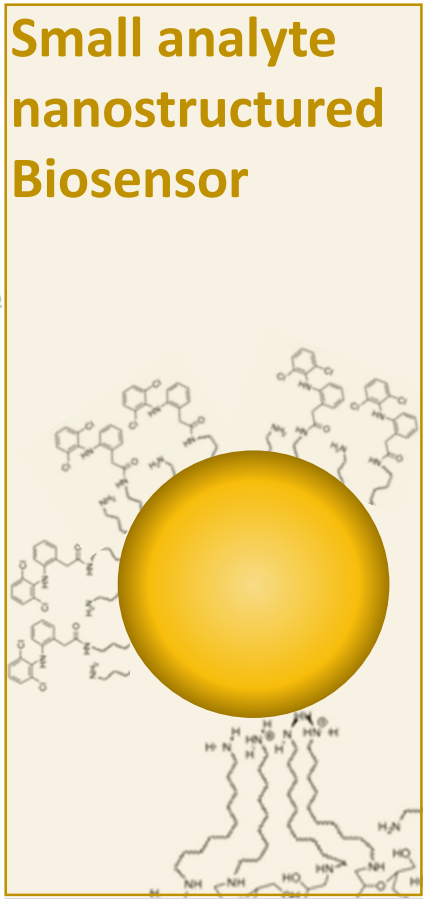


1
2
3
4
5
6
7
8
9
10
11
12
13
14
15
16
17
18
19
20
21
22
23
24
25
26
27
28
29
30
31
32
33
34
35
36
37
38
39
40
41
42



AuNP
Controlled
assembly

TEM SEM
IR QCM-D



© Paragon Plus Environment